



1 Negentropy anomaly analysis of the borehole strain associated with the Ms 8.0
2 Wenchuan earthquake

3 Kaiguang Zhu^{1,2*}, Zining Yu^{1,2}, Chengquan Chi^{1,2}, Mengxuan Fan^{1,2} and Kaiyan Li^{1,2}

4 ¹ College of Instrumentation and Electrical Engineering, Jilin University, China

5 ² Key Laboratory of Geo-Exploration Instrumentation, Ministry of Education, Jilin University, China

6 **Abstract:** A large earthquake of 8.0 magnitude occurred on 12 May 2012, 14:28 UTC, with the
7 epicenter in Wenchuan. To investigate the pre-earthquake anomalous strain changes, negentropy is
8 introduced to borehole strain data at Guza station, approximated by skewness and kurtosis revealing
9 the non-Gaussianity of recorded fluctuations. We separate the negentropy anomalies from the
10 background by Otsu's method and accumulate the anomaly frequency in different scales. The results
11 show the long-scale cumulative frequency of negentropy anomalies follows a sigmoid behaviour,
12 while the inflection point of the fitting curve is close to the occurrence of the earthquake. For the
13 short-scale analysis before the earthquake, there are two cumulative acceleration phases
14 corresponding to the two crustal stress releases, indicating the preparation process of the Wenchuan
15 earthquake. We consider that negentropy exhibits potential for the analysis of earthquake precursor
16 anomalies.

17 **Keywords:** Negentropy anomaly, Otsu's thresholding, Cumulative frequency, Wenchuan earthquake

18 1. Introduction

19 Changes in crustal deformation fields over time have preceded at least some large earthquakes
20 (Thatcher, W. et al., 1981), such as the 2011 Tohoku earthquake (Hitoshi Hirose, 2011) and the
21 Ruisui earthquake in Taiwan in 2013 (Canitano A. et al., 2015). Borehole strain data, which record
22 the direct crustal changes, provide an opportunity to investigate preparation process prior to
23 earthquakes (Linde et al., 1996, Hsu, Y.-J. et al. 2015).

24 Various methods are used in identifying borehole strain anomalies based on large amount of
25 monitoring data. Experienced scholars extract borehole strain anomalies by discriminating patterns
26 of waveform behaviors compared to those during the normal stage (M.J.S. Johnston et al., 2006, Chi
27 S. L. et al., 2014). In the time domain, Qiu Z. H. et al. (2010) identified abnormal strain changes by
28 overrun rate and wavelet decomposition for the Wenchuan earthquake. While in the frequency



29 domain, Qi L. et al. (2011) thought the signal with a period of 10 to 60 minutes might be anomalies
30 through S-transform compared with the background signal. In addition, statistical methods are
31 proved effective in distinguishing borehole strain anomalies with regard to large earthquakes, such as
32 principal component analysis (Zhu K. G. et al., 2018) and correlation coefficients along with the
33 consistency relation (Kong X. et al., 2018).

34 The probability distribution function (PDF) of observation data is also an informative way of
35 extracting potential anomalies contained in earthquake generation processes. P. Manshour et al.
36 (2009) extracted variance anomalies of the probability density of the Earth's vertical velocity
37 increments, and successfully found a pronounced transition from Gaussian to non-Gaussian prior to
38 12 moderate and large earthquakes. Before the Wenchuan earthquake, the high-frequency fluid
39 observational data deviated from Gaussian distributions at 16 water level and 14 water temperature
40 stations (Sun X. L. et al., 2016).

41 Rather than the whole PDF, often its moments are utilized, moments may be estimated quite
42 reliably from relatively small amounts of data (Sattin, F. et al., 2009). In 2016, Chen H. J. et al.
43 applied skewness and kurtosis (the third- and fourth-order moments) of the geoelectric data to pick
44 up non-Gaussian anomalies to predict impending large earthquakes in Taiwan. On the other hand, for
45 turbulent or disordered systems, the non-Gaussian distribution of time series in skewness-kurtosis
46 domain attracts attention. Observation data series from various fields of geophysics indicate that a
47 parabolic relation between skewness and kurtosis holds in fields such as seismology (M. Cristelli, et
48 al., 2012), oceanography (Sura, P. et al., 2008) and atmospheric science (A. Maurizi, 2006).

49 Hence, it is implied that possible precursor anomalies deviate from Gaussian distribution during
50 earthquake preparation processes. In this study, the negentropy is applied to borehole strain at Guza
51 station associated with the Wenchuan earthquake, approximated by skewness and kurtosis revealing
52 the non-Gaussianity of borehole fluctuations. Subsequently we study the extracted negentropy
53 anomalies in different scales to investigate correlations with crustal deformation.

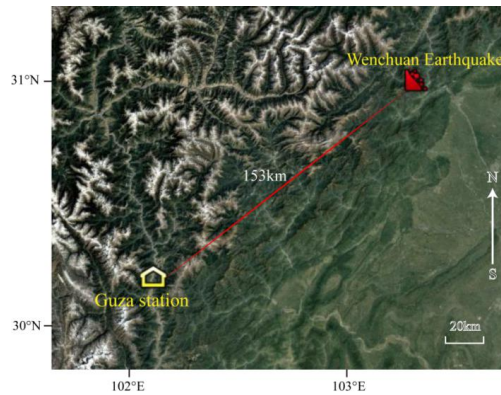
54 2. Observation

55 YRY-4 borehole strainmeters, which are designed to record continuous deformation occurring
56 over periods of minutes to years, have been deployed at depths of dozens of metres at more than 40



57 terrain-sensitive locations within China. These strainmeters are capable of resolving strain changes
58 of less than one-billionth. The data sampling rate is once per minute.

59 The study period is from January 1, 2007, to June 30, 2009. The object of the study is the
60 Wenchuan Ms 8.0 earthquake in the region, which is shown in Fig. 1.



61
62 Fig. 1. Location map showing the epicentre of the Wenchuan earthquake epicentre and the Guza station. The
63 Wenchuan earthquake occurred at 14:28:04 on May 12, 2008 (UTC+8). The magnitude of the earthquake was Ms
64 8.0, and the focal depth was approximately 14 km. The epicentre was located in Wenchuan County, Sichuan
65 Province, at 31.01°N, 103.42°E.

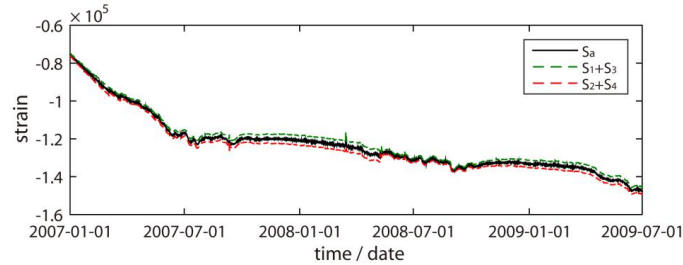
66 Because the four gauges of the YRY-4 borehole strainmeter are arranged at 45° intervals, this
67 design has improved its self-consistency. This arrangement produces four observation values: S_i ,
68 ($i=1, 2, 3, 4$) (Qiu et al., 2013a). The self-consistency as shown in equation (1), which can be used to
69 test the reliability of the data among the four gauges.

$$70 \quad S_1 + S_3 = S_2 + S_4 \quad (1)$$

71 In practical application, the higher the correlation between both sides of the equation (1), the
72 more reliable the data. Generally, we use S_a for the areal strain in describing the subsurface strain
73 state of the observation area as shown in equation 2 (Qiu et al., 2013a):

$$74 \quad S_a = (S_1 + S_2 + S_3 + S_4) / 2 \quad (2)$$

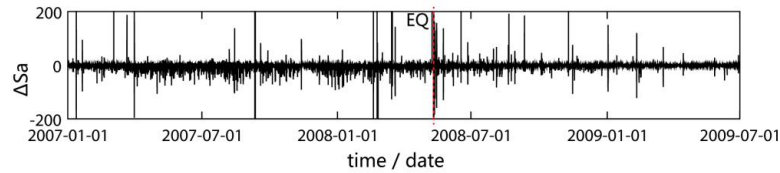
75 The borehole strain is highly consistent among the four gauges at the Guza station (Qiu, et al.,
76 2009), as shown in Fig. 2.



77
 78

Fig. 2. Self-consistency of the borehole strain at Guza from January 1, 2007, to June 30, 2009.

79 We first calculate the difference in the data because in the borehole strain data, the change in the
 80 strain is a concern (Li Jinwu et al., 2014). We then remove the components associated with the solid
 81 tide frequencies through a daily harmonic analysis. The remaining high-frequency signals are shown
 82 in Fig. 3.



83

84 Fig. 3. High-frequency areal strain after removing harmonic information at Guza from January 1, 2007 to June 30,
 85 2009.

86 3. Methodology

87 3.1 Negentropy and non-Gaussianity

88 The entropy-based negentropy is a statistically justified measure of non-Gaussianity (A.
 89 Hyvarinen, et al., 2000). The entropy of a random variable $X = \{x_1, x_2, \dots, x_i, \dots\}$ is defined as

$$90 \quad H(X) = -\sum_i P(X = x_i) \log P(X = x_i) \quad (3)$$

91 where P is the probability density function. Entropy measures the randomness of a random variable.
 92 The Gaussian random variable has the largest entropy of all other random variables with equal
 93 variance (T.M. Cover et al., 1991). The definition of negentropy is given by

$$94 \quad J(X) = H(X_{gauss}) - H(X) \quad (4)$$

95 in which X_{gauss} is a Gaussian random variable with the same mean and covariance matrix as X . The
 96 entropy of a Gaussian random variable can be estimated by



97
$$H(X_{\text{gauss}}) = \frac{1}{2} \log |\det \Sigma| + \frac{n}{2} (1 + \log 2\pi) \quad (5)$$

98 where n is the dimension of the variable, and Σ is its covariance matrix.

99 However, the theoretical calculation of negentropy also depends on the prior probability density
100 of random variables and other information that is difficult to determine accurately. In practical
101 applications, higher order statistics (HOS) and density polynomial expansion are usually used to
102 approximate one-dimensional negentropy (Jones and Sibson, 1987). The approximation results are as
103 follows:

104
$$J(x) \approx \frac{1}{12} \text{skewness}^2(X) + \frac{1}{48} \text{kurtosis}^2(X) \quad (6)$$

105 This definition suggests that any deviation from a Gaussian distribution will increase the
106 negentropy $J(x)$. The skewness and kurtosis are the third- and fourth-order statistics, respectively,
107 which are defined as

108
$$\text{skewness}(X) = \frac{\mu_3}{\sigma^3} = \frac{E[(X - \mu)^3]}{E[(X - \mu)^2]^{3/2}} \quad (7)$$

109 and

110
$$\text{kurtosis}(X) = \frac{\mu_4}{\sigma^4} = \frac{E[(X - \mu)^4]}{E[(X - \mu)^2]^2} - 3 \quad (8)$$

111 where μ is the mean of X and σ is the standard deviation of X . Skewness is a measure of
112 asymmetry in a PDF. A symmetric distribution has zero skewness. Kurtosis is a measure of the
113 heaviness of the tails. Distributions that are more outlier-prone than the normal distribution have
114 kurtosis values greater than zero.

115 Moreover, the relation between the skewness and kurtosis is universal, they approximately align
116 along a quadratic curve (Sattin, F., et al., 2009):

117
$$\text{kurtosis}(X) = A \cdot \text{skewness}^2(X) + B \quad (9)$$

118 This relation is trivial in a Gaussian fluctuating system; it reduces to a fixed mass around zero
119 (skewness= 0 and kurtosis= 0). In a turbulent environment where fluctuating quantities obey
120 non-Gaussian statistics, the moments obey the above relation.

121 3.2 Otsu's thresholding method



122 To solve the negentropy anomaly detection problem, we designed a simple thresholding
 123 hypothesis test using the Otsu method (Otsu, 1979) that provides an optimal separation between
 124 background and seismic-related activities. For any given value k , we can separate the previously
 125 calculated $J(x)$, as shown in equation (6), into the following two classes:

$$126 \quad \begin{aligned} C_0(k) &= \{J(x) \leq k\}, \\ C_1(k) &= \{J(x) > k\}. \end{aligned} \quad (10)$$

127 Using these classes, the weighted average value $\mu_T(x)$ of $J(x)$ can be expressed as follows:

$$128 \quad \begin{aligned} \mu_T(x) &= \lambda_0(k)\mu_0(x; k) + \lambda_1(k)\mu_1(x; k), \\ \lambda_0(k) + \lambda_1(k) &= 1. \end{aligned} \quad (11)$$

129 where $\mu_0(x; k), \mu_1(x; k)$ are the mean values of the class $C_i(k)$, $i=1, 2$, and $\lambda_i(k)$ is the
 130 percentage of points belonging into each class. Following the thresholding scheme of Otsu (1979),
 131 we define the following cost function:

$$132 \quad \begin{aligned} \sigma_B^2(k) &= \lambda_0(k)(\mu_0(x; k) - \mu_T(x; k))^2 + \lambda_1(k)(\mu_1(x; k) - \mu_T(x; k))^2 \\ &= \lambda_0(k)\lambda_1(k)(\mu_1(x; k) - \mu_0(x; k))^2 \end{aligned} \quad (12)$$

133 where σ_B^2 is the within-class variance of negentropy. Then, by finding the k^* value searching for k
 134 when σ_B^2 becomes the maximum

$$135 \quad k^* = \arg \max_k \sigma_B^2(k) \quad (13)$$

136 the optimal value k^* here separates the background set and anomaly set.

137 In this test, our initial assumption is that the sliding window is composed of a Gaussian signal of
 138 non-seismic-related activities. When our test negentropy exceeds the critical value k^* , this initial
 139 hypothesis is not valid, and the alternative is true, indicating the presence of a negentropy anomaly
 140 within the window.

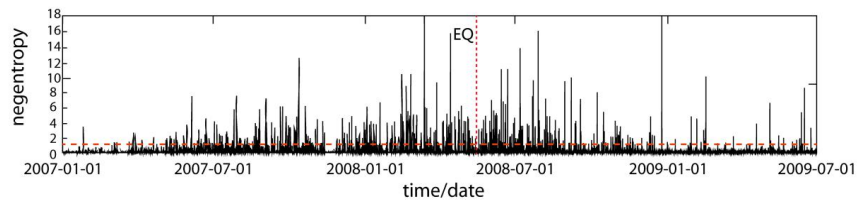
141 4. Results

142 According to the empirical hypothesis that geophysical signals deviate from the Gaussian
 143 distribution when they record seismic-related activities, and based on the results of previous studies,
 144 we conduct the following investigation.

145 4.1 Extracting negentropy anomalies

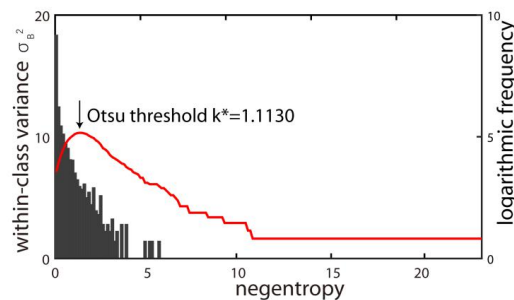


146 As the negentropy is calculated using a 2-hour long sliding window, we assume that it reaches
147 the maximum values when the time window contains anomalies from seismic-related activities. The
148 negentropy during the study period is shown in Fig. 4.



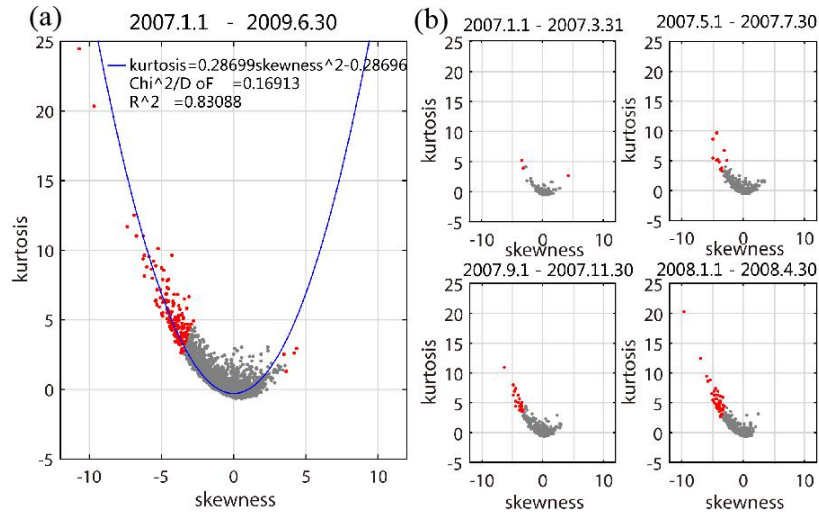
149
150 Fig. 4. Negentropy at Guza from January 1, 2007, to June 30, 2009. The red dotted, horizontal line is the optimal
151 threshold k^* calculated by Otsu's method.

152 The within-class variance σ_B^2 and negentropy value distribution are compared in Fig. 5.
153 According to equations (10) to (13), when $k^*=1.1130$, σ_B^2 reaches its maximum. Therefore, the
154 negentropies were separated by k^* into the quasi-Gaussian background and non-Gaussian anomalies
155 from 2007 to 2009.



156
157 Fig. 5. Within-class variance σ_B^2 of the negentropy (red line) and negentropy histogram

158 In the skewness-kurtosis domain, the statistical relationship of the borehole areal strain is
159 consistent with parabolic behaviour as described in equation (9)(Fig 6(a)), verifying that the
160 turbulent system of borehole strain is significantly non-Gaussian during the study period. However,
161 the extracted negentropy anomalies are clustered strongly on the left side of the parabola, which
162 could be a signature of crustal deformation related to the earthquake. Here, there are four points on
163 the right side; one occurred in early 2007, and the others occurred after the earthquake. Therefore,
164 we will not discuss them in the following.



165
166 Fig. 6. Negentropy distributions in the skewness-kurtosis domain in (a) January 1, 2007, to June 30 2009, and (b)
167 four shorter periods before the earthquake. Red denotes that the negentropy is greater than k^* , and grey indicates
168 that the negentropy less than k^* . The blue curve is the quadratic fit with the a 95% confidence.

169 In addition, as shown in Fig. 6(b), at times far from the earthquake, the negentropy distribution
170 is basically Gaussian in the skewness-kurtosis domain. However, at times closer to the earthquake,
171 the distribution gradually begins to show non-Gaussianity, with more negentropy anomalies
172 appearing on the left side of the parabola. While in 2008, almost all of the negentropy present
173 left-skewed.

174 These phenomena prompt us to study the origin of this left-skewed distribution and its possible
175 correspondence with the seismogenic process.

176 4.2 Negentropy anomaly frequency accumulation

177 The transition of negentropy anomalies in the skewness-kurtosis domain is quantified as the
178 change of the anomaly frequency per unit time through a logarithmic-linear model.
179 Logarithmic-linear models are often used of interest to estimate the expected frequency of the
180 response variable at the original scale for a new set of covariate values, such as in the famous
181 Gutenberg-Richer law, in which a linear relationship exists between the logarithm of the cumulative
182 number of seismic events of magnitude M or greater versus the magnitude M (Gutenberg and Richer,
183 1954).

184 The logarithmic-linear regression model is proposed as



185
$$\log N = \beta_1 \times k_j + \beta_0 + \varepsilon \quad (14)$$

186 where k_j takes different threshold values according to the $J(x)$ values, N is the number of
 187 occurrences in which J is greater than or equal to the threshold k_j , β_0 and β_1 are the regression
 188 coefficients, where a lower slope β_1 indicates that there are more higher J values, implying there
 189 are more anomalies at that moment, and ε is the random error that represents the model uncertainty.

190 We use the logarithmic-linear model to solve the relationship between the negentropy anomaly
 191 frequency and different thresholds each day using the ordinary least squares method (OLS) method.
 192 Afterwards, an optimal threshold k^* , calculated by the Ostu method, is chosen for all models, where

193
$$N_j(t) = \exp(\beta_1(t) \times k^* + \beta_0(t) + \varepsilon(t)) \quad (15)$$

194 and the $N_j(t)$ under the threshold k^* is shown in Fig. 7. The model theoretically solves the
 195 problem of selecting the length of the time window. In addition, the estimated $N_j(t)$ is considered
 196 as the expected frequency of anomalies.

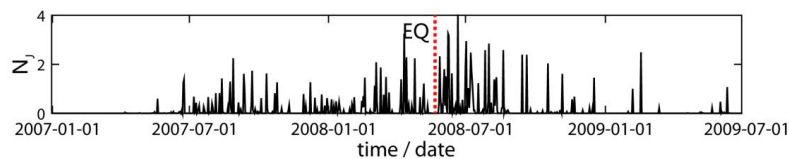
197 The goodness of fit for each logarithmic-linear model was evaluated using analysis of

198
$$R^2 = 1 - \frac{\sum_{i=1}^n (N_i - \hat{N}_i)^2}{\sum_{i=1}^n (N_i - \bar{N}_i)^2} \quad (16)$$

199 and the root-mean-squared error

200
$$RMSE = \sqrt{\frac{\sum_{i=1}^n (N_i - \hat{N}_i)^2}{n}} \quad (17)$$

201 The R^2 and $RMSE$ values in the study period (912 days) show that the logarithmic-linear
 202 relationship can explain the relationship between the negentropy anomaly frequency and different
 203 thresholds. The mean of R^2 is 0.9695, which is close to 1, and the variance of R^2 is 0.0435. The
 204 mean and variance of the $RMSE$ are also small (0.1098 and 0.1301, respectively).



205

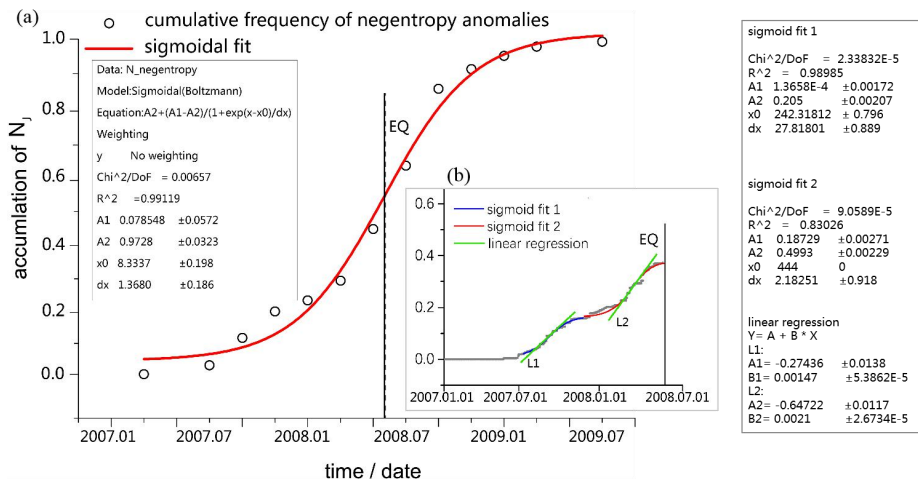
206 Fig. 7. Estimated expected frequency N_j under the optimal threshold k^*

207 In general, accumulated value of a typical random process usually has an linear increase. The
 208 negentropy cumulative frequency of the study period is shown in Fig. 8. We not only do a long-scale



209 analysis of the whole earthquake process, but also carry out a short-scale analysis of the
 210 pre-earthquake process.

211 For the entire earthquake process, a two-month long sliding window is selected for
 212 accumulation as shown in Fig. 8(a). Beginning in July 2007, the negentropy anomalies gradually
 213 accumulated. In particular, we find more frequent negentropy anomalies in 2008 as the earthquake
 214 approaches, and less frequent anomalies after, so a sigmoid function is used to fit the acceleration,
 215 before the earthquake and the deceleration after. According to De Santis, A. et al. (2017), inflection
 216 point in this function is a reasonable estimation of the time of the significant change in the critical
 217 dynamical system. Our calculation shows that the inflection point x_0 of the optimal fitting is 8.3337,
 218 which is surprisingly close to the actual time (8.3871) of the Wenchuan earthquake after conversion.
 219 Thus, the earthquake moment is proved to be a critical time during the whole Wenchuan earthquake
 220 process.



221
 222 Fig. 8. (a) Results of the long-scale negentropy anomaly frequency for the Wenchuan earthquake at Guza station
 223 from January 1, 2007, to June 30, 2009. Each circle represents an anomaly negentropy for 2 months. The
 224 cumulative frequency of negentropy anomaly is represented. The earthquake day is represented as a vertical solid
 225 line. The red line is a sigmoidal fit that underlines a critical point (vertical dashed line) is close to the occurrence of
 226 the earthquake. (b) Results of the short-scale negentropy anomaly frequency prior to the earthquake, every grey
 227 point is an anomaly for one day, the blue and red lines are two segment sigmoid fit results. Two green lines
 228 represent the liner regression for the two phases, the first phase slope is 0.00147, the second one is 0.0021.



229 When we narrowed the accumulated window to one day, we observed two negentropy anomalies
230 before the earthquake as shown in Fig. 8(b). The first anomaly frequency increase occurred from
231 August to October 2007. In March 2008, there was a second phase of anomaly increase, and the
232 cumulative frequency then slowly increased to a plateau period near the time of the earthquake.
233 These two phases prior to the earthquake are also approximated with sigmoid functions. In order to
234 further compare the anomalies of the two phases, we use linear regression to fit the central part of the
235 two sigmoid curves. We find that the second acceleration is greater than the first acceleration. We
236 think the accumulations of these two negentropy anomalies may be an indication of crustal activity
237 before the Wenchuan earthquake.

238 5. Discussion and Conclusion

239 Previous studies for the Wenchuan earthquake are consistent with our findings. Wang (2018)
240 concluded that an apparent stress change occurred after June 2007 based on multiple focal
241 mechanisms. Likewise, we did not find negentropy anomalies in the first six months of 2007. In the
242 large-scale analysis, we show that the cumulative frequency of negentropy anomalies follows the a
243 power-law behaviour approaching a critical time that is close to the earthquake time, and then
244 recovers as a typical recovery phase after the earthquake This process is consistent with the empirical
245 phenomena before and after earthquakes, which is also similar with a potential earthquake precursory
246 pattern in magnetic data from Swarm satellites by A. De Santis (2017) for the 2015 Nepal event.

247 Qiu (2009) and Chi (2014) speculated that the areal strain indicates that the integrity of the
248 medium around the borehole at the Guza station began to change significantly after August 2007,
249 because the continuity of the medium in the source region of the Wenchuan earthquake was
250 gradually deformed during the nucleation process. In our short-scale analysis, negentropy anomalies
251 also present a acceleration in August 2007. The second acceleration in March 2008 is also consistent
252 with the occurrence of a phase measured by GPS (Jiang Z. S., 2009), in which the elastic
253 deformation of the crust reaches its limit, and the deformation is resisted in the seismogenic region
254 before the earthquake.

255 More importantly, we speculate that the two accelerations of the cumulative negentropy
256 anomaly corresponding to two stress releases. Ma Jin (2014) proposed the deformation
257 characteristics in the sub-instability stage of faults before earthquakes based on different experiments



258 and several earthquakes. Fault zones contain relatively weak and relatively strong parts. The former
259 is the area where strain release begins, while the latter is the stress locking part and the beginning of
260 rapid instability (Noda et al., 2013). She thinks accelerated expansion of the strain release zone in
261 fault zone is a sign of entering the inevitable earthquake stage. There are two instabilities before
262 earthquakes, the former is related to the release of weak parts, and the latter is related to the rapid
263 release of strong parts of the fault during strong earthquakes. The accelerated expansion of the
264 former promotes the occurrence of the latter.

265 We speculate that the two negentropy anomaly accelerations may represent the two instabilities
266 associated with the Wenchuan earthquake. The first corresponds to the start of strain release and the
267 second larger one corresponds to the acceleration of instability, indicating that strong earthquakes are
268 likely to occur.

269 In our work, the extracted negentropy anomalies of the short-period signal of borehole areal
270 strain based on Otsu's thresholding associated with the Wenchuan earthquake are analyzed. A
271 logarithmic-linear model is proposed to estimate the expected frequency of the left-skewed
272 negentropy anomaly for everyday, and the evolution processes of the negentropy anomaly frequency
273 are studied in both long- and short-scale during the study period. We consider the negentropy
274 anomalies corresponding to crustal stress changes, which may be a reflection of the subsurface
275 medium and faults activities in the focal area associate with the Wenchuan earthquake. Moreover, we
276 may be able to ensure that the negentropy has great potential in the study of earthquake precursors.

277 **Acknowledgements**

278 The authors are appreciative of the Key Laboratory of the Geo-Exploration Instrumentation of
279 Ministry of Education in Jilin University of China. Moreover, the authors are grateful to Professor
280 Zehua Qiu for his guidance and helpful suggestions. This research was supported by the Institute of
281 Crustal Dynamics, China Earthquake Administration (Grant No.3R216N620537).

282 **References**

283 A. Hyvarinen, E. Oja. Independent component analysis: algorithms and applications, Neural Net.
284 13:411-430, 2000.

285 A. Maurizi. On the dependence of third- and fourth-order moments on stability in the turbulent
286 boundary layer. Nonlinear Processes in Geophysics. 13(1):119-123, 2006.



- 287 Canitano, A., Hsu, Y.J., Lee, H.M. et al. Near-field strain observations of the October 2013 Ruisui,
288 Taiwan, earthquake: source parameters and limits of very short-term strain detection, *Earth,*
289 *Planets and Space*, 67(125), 2015.
- 290 Chen H.J., Chen C.C. Testing the correlations between anomalies of statistical indexes of the
291 geoelectric system and earthquakes. *Nat Hazards* 84(2): 877-895, 2016.
- 292 Chi S.L., et al. Failure of self-consistent strain data before Wenchuan, Ludian and Kangding
293 earthquake and its relation with earthquake nucleation. *Recent Developments in World*
294 *Seismology*. 12:3-13, 2014.
- 295 De Santis, A., et al. "Potential earthquake precursory pattern from space: The 2015 Nepal event as
296 seen by magnetic Swarm satellites." *Earth and Planetary Science Letters* 461: 119-126, 2017.
- 297 Gutenberg, B., Richer, C.F. *Seismicity of the Earth and Associated Phenomena*. Princeton University
298 Press, Princeton, NJ, 1954.
- 299 Hirose, H. Tilt records prior to the 2011 off the Pacific coast of Tohoku Earthquake, *Earth Planet and*
300 *Space*, 63(7): 665-658, 2011.
- 301 Hsu, Y.-J., et al. Revisiting borehole strain, typhoons, and slow earthquakes using quantitative
302 estimates of precipitation-induced strain changes. *Journal of Geophysical Research: Solid Earth*,
303 120(6): 4556-4571, 2015.
- 304 Jones, M. C., and R. Sibson. What is projection pursuit?: *Journal of the Royal Statistical Society*
305 *Series A*, 150, 1-37, 1987.
- 306 Jiang Z.S, Fang Y., Wu Y.Q, et al. The dynamic process of regional crustal movement and
307 deformation before Wenchuan Ms8.0 earthquake. *Chinese J. Geophys.* (in Chinese), 52
308 (2):505-518, 2009.
- 309 Kong, X., et al. A Detection Method of Earthquake Precursory Anomalies Using the
310 Four-Component Borehole Strainmeter. *Open Journal of Earthquake Research* 07(02): 124-140,
311 2018.
- 312 Linde, A. T., M. T. Gladwin., M. J. S. Johnston., R. L. Gwyther and R. G. Bilham. A slow
313 earthquake sequence on the San Andreas fault. *J. Nature*. 383. 65–68, 1996.
- 314 Li J. W., Qiu Z. H. Analysis on strain tidal factor observed borehole strainmeters, *Progress in*
315 *Geophysics*, 29(5): 2013-2018, 2014.



- 316 Ma Jin, Guo Yan-shuang. Accelerated synergism prior to fault instability evidence from laboratory
317 experiments and an earthquake case, *Seismology and Geology*, 36(3): 547-560, 2014.
- 318 M. Cristelli, A. Zaccaria and L. Pietronero. Universal relation between skewness and kurtosis in
319 complex dynamics, *Physical Review E*, vol. 85(6):066-108, 2012.
- 320 M. J. S. Johnston, Y. Sasai, G. D. Egbert, R. J. Mueller. Seismomagnetic Effects from the
321 Long-Awaited 28 September 2004 Ms6.0 Parkfield Earthquake. *Bulletin of the Seismological*
322 *Society of America*, 96 (4B): 206-220, 2006.
- 323 Noda H, Nakatani M, Hori T. Large nucleation before large earthquakes is sometimes skipped due to
324 cascadeup Implications from a rate and state simulation of faults with hierarchical asperities. *J*
325 *Geophys Res Solid Earth*, 118: 2924-2952, 2013.
- 326 Otsu, N. A threshold selection method from gray-level histograms: *IEEE Transactions on Systems,*
327 *Man and Cybernetics*, 9:62-66, 1979.
- 328 P. Manshour, S. Saberi, Muhammad Sahimi, J. Peinke, Amalio F. Pacheco, and M. Reza Rahimi
329 Tabar. Turbulencelike Behavior of Seismic Time Series. *Phys. Rev. Lett.* 102(1):014101, 2009.
- 330 Qi L., Jing Z. Application of S transform in analysis of strain changes before and after Wenchuan
331 earthquake. *J. Journal of Geodesy and Geodynamics*. 4: 003, 2011.
- 332 Qiu Z H. et al. Strain changes of four-component borehole strain network before the Wenchuan
333 earthquake. *Journal of Geodesy and Geodynamics*, 29 (1): 1-5, 2009.
- 334 Qiu Z.H., Zhang B H., Chi S L., et al. Abnormal strain changes observed at Guza before the
335 Wenchuan earthquake. *J. Science China Earth Sciences*. 54(2): 233-240, 2010.
- 336 Qiu Z.H., Tang L., Zhang B., et al. In situ calibration of and algorithm for strain monitoring using
337 four gauge borehole strainmeters (FGBS). *J. Journal of Geophysical Research: Solid Earth*.
338 118(4): 1609-1618, 2013.
- 339 Sattin, F., et al. About the parabolic relation existing between the skewness and the kurtosis in time
340 series of experimental data. *Physica Scripta* 79(4), 2009.
- 341 Sun X L, Wang, G C, Yan R. Extracting high-frequency anomaly information fluid observational
342 data: a case study of the Wenchuan Ms8.0 earthquake of 2008. *Chinese J. Geophysics*.
343 59(5):1673-1684, 2016.
- 344 Sura, P. and P. D. Sardeshmukh. A Global View of Non-Gaussian SST Variability. *Journal of*
345 *Physical Oceanography* 38(3): 639-647, 2008.



- 346 T.M. Cover, J.A. Thomas. Elements of Information Theory, Wiley, New York, 1991.
- 347 Thatcher, W., and T. Matsuda. Quaternary and geodetically measured crustal movements in the
348 Tokai District, Central Honshu, Japan, J. Geophys. Res., 86(B10), 9237–9247, 1981.
- 349 Wang K Y, Guo Y S, Feng X. D. Sub-instability stress state prior to the 2008 Wenchuan earthquake
350 from temporal and spatial stress evolution. Chinese J. Geophys. (in Chinese), 61(5): 1883-1890,
351 2018.
- 352 Zhu, Kaiguang, et al. Extracting borehole strain precursors associated with the Lushan earthquake
353 through principal component analysis. Annals of Geophysics, 61(4):1593-5213, 2018.